Materials for light-induced water splitting: In situ controlled surface preparation of GaPN epilayers grown lattice-matched on Si(100)

Oliver Supplie,[1,2,a)] Matthias M. May,[1,2] Helena Stange,[1,2] Christian Höhn,[1] Hans-Joachim Lewerenz,[1,3] and Thomas Hannappel[1,4]

[1)] *Helmholtz-Zentrum Berlin, Institute Solar Fuels, Hahn-Meitner-Platz 1, 14109 Berlin, Germany*

[2)] *Humboldt-Universität zu Berlin, Institut für Physik, Newtonstr. 15, 12489 Berlin, Germany*

[3)] *California Institute of Technology, Joint Center for Artificial Photosynthesis, 1200 East California Boulevard, Pasadena, CA 91125, USA*

[4)] *Technische Universität Ilmenau, Institut für Physik, Gustav-Kirchhoff-Str. 5, 98684 Ilmenau, Germany*

Energy storage is a key challenge in solar-driven renewable energy conversion. We promote a photochemical diode based on dilute nitride GaPN grown lattice-matched on Si(100), which could reach both high photovoltaic efficiencies and evolve hydrogen directly without external bias. Homoepitaxial GaP(100) surface preparation was shown to have a significant impact on the semiconductor-water interface formation. Here, we grow a thin, pseudomorphic GaP nucleation buffer on almost single-domain Si(100) prior to GaPN growth and compare the $GaP_{0.98}N_{0.02}$/Si(100) surface preparation to established P- and Ga-rich surfaces of GaP/Si(100). We apply reflection anisotropy spectroscopy to study the surface preparation of $GaP_{0.98}N_{0.02}$ *in situ* in vapor phase epitaxy ambient and benchmark the signals to low energy electron diffraction, photoelectron spectroscopy, and x-ray diffraction. While the preparation of the Ga-rich surface is hardly influenced by the presence of the nitrogen precursor UDMH, we find that stabilization with UDMH after growth hinders well-defined formation of the V-rich $GaP_{0.98}N_{0.02}$/Si(100) surface. Additional features in the reflection anisotropy spectra are suggested to be related to nitrogen incorporation in the GaP bulk.

I. INTRODUCTION

Conversion of sunlight into electric energy in solar cells nowadays reliably reaches photovoltaic (PV) efficiencies of about 20 % at commercially available roof-mounted modules and world-record efficiencies above 44 % were already demonstrated in the laboratory for terrestrial concentrator PV solar cells.[1,2] Energy storage and renewable fuel production, however, remain the key challenges to gain independence from fossil fuels and intermittent irradiation. Photoelectrolysis of water converts sunlight into chemical energy, stored in bonds of molecular hydrogen, which can also be further converted into renewable fuels such as methanol or synthethic hydrocarbons.[3] In search for optimum materials for light-induced unassisted water splitting, both bulk and surface properties are crucial: the bulk has to provide a suitable bandgap, adequate absorption and charge carrier transport whereas the surface needs to exhibit proper energy band alignment, promote carrier transport to the liquid and remain stable. In particular, the band alignment of GaP(100) is suitable for both direct hydrogen[4] and oxygen evolution, while the indirect, large bandgap reduces the absorption efficiency.[5] Tandem approaches, in contrast, promise high solar-to-hydrogen efficiencies, with a maximum for 1 eV bandgap bottom cells,[6,7] which favors silicon as active substrate. Thin GaP epilayers free of anti-phase disorder can be grown pseudomorphic with *in situ* control on double-stepped Si(100) substrates in metalorganic vapor phase epitaxy (MOVPE).[8–10] Already small amounts of nitrogen incorporation enable lattice-matched growth of $GaP_{0.98}N_{0.02}$ on Si(100) with suitable bandgaps for direct photoelectrolysis[6] and increased stability towards the electrolyte.[11] Applying *in situ* reflection anisotropy spectroscopy (RAS), we recently showed that the formation of the interface between GaP(100) and water depends highly on the atomic structure of the GaP surface prior to exposure[12]. RA spectra of P-rich and Ga-rich GaP(100) surfaces are well-understood both in theory[13,14] and experiment,[15–17] which enables precise *in situ* control during MOVPE preparation. Pseudomorphic GaP/Si(100) surfaces can be prepared analogously to GaP(100) regarding atomic order.[10] Though *in situ* control is even more important during growth of ternary compounds, to our knowledge RAS has not yet been applied to study the influence of nitrogen during GaPN/Si(100) growth and surface preparation.

In this article, we compile the band alignment of III-V/IV heterostructures relative to the redox potential of water and suggest a photochemical diode based on dilute nitride GaPN grown lattice-matched on Si(100) for efficient light-induced water splitting. We compare the MOVPE-preparation as well as *in situ* RA spectra of group–V-rich and Ga-rich GaPN/Si(100) surfaces to established GaP/Si(100) processing. Regarding atomic order and cleanliness, we benchmark the *in situ* spectra to low energy electron diffraction (LEED) as well as x-ray photoelectron spectroscopy (XPS) after contamination-free transfer[18] to ultrahigh vacuum (UHV) and apply high-resolution x-ray diffraction (XRD) as a measure for the nitrogen incorporation into the GaP bulk.

[a)] Electronic mail: oliver.supplie@helmholtz-berlin.de

II. EXPERIMENTAL

Samples were prepared in an AIX-200 horizontal MOVPE reactor modified with a dedicated UHV-transfer system[18]. Pd-purified H_2 was used as process gas and temperatures were measured with a thermocouple placed inside the susceptor. The whole process was monitored *in situ* with a LayTec EpiRAS-200 spectrometer aligned so that

$$\frac{\Delta r}{r} = 2\frac{r_{[0\bar{1}1]} - r_{[011]}}{r_{[0\bar{1}1]} + r_{[011]}} \quad , \tag{1}$$

where $r(\lambda)$ denotes the complex index of reflection[19]. A baseline accounting for contributions of the optical components was substracted from all spectra shown here.

Almost single-domain, (1×2)-reconstructed Si(100) substrates with 2° misorientation towards [011] were prepared as in Ref.[8] prior to pulsed GaP nucleation and GaP growth using the precursors tertbutylphoshine (TBP) and triethylgallium (TEGa). The growth time was 70 s for the GaP/Si(100) reference sample and 34 s for the GaPN/GaP/Si(100) sample. Both GaP layers were prepared P-rich[10] and for the latter sample, GaPN was subsequently grown for 34 s at 595 °C using 1,1-dimethylhydrazine (UDMH) at UDMH:TBP and TBP:TEGa ratios of 1.4 and 13, respectively, aiming at about 2 % N incorporation for lattice-matching to Si. At first, both group V precursors were offered during cooling to stabilize the surface prior to the "P-rich" annealing step. The samples were transferred to UHV, where XPS (Specs Focus 500 and Phoibos 100) and LEED (Specs ErLEED 100-A) were accessible via a mobile UHV shuttle in order to check the atomic order at the surface and the cleanliness. Both samples were then transferred back into the MOVPE reactor, where the Ga-rich surfaces were prepared with RAS *in situ* control by annealing in hydrogen at 700 °C without precursor supply[10]. Subsequently, the samples were again measured by LEED and XPS. A third sample was prepared similarly, but without UDMH supply during cooling after GaPN growth. High-resolution x-ray diffraction (XRD) was measured using a Panalytical X'PertPro diffractometer.

III. GAPN/SI-BASED PHOTOCHEMICAL DIODE

State of the art electrolysers, currently tested in the field for use in sustainable hydrogen production, are mostly dark electrolysers which are powered by external power supply, efficient only at large scale, and involve non-abundant metals and catalysts. Multijunction approaches for direct, "wireless" photoelectrolysis aim at combining absorption of sunlight and unbiased water splitting into one single device, as pioneered already in the 1980's[20] and demonstrated for Si triple junction cells[21,22]. Such a device differs from "standard" solar cells in many ways: (1) Given the redox potential of 1.23 eV and required overpotentials, generation of a minimum photovoltage of about 1.8 V is necessary to split water[23]. Tandem devices are feasible to achieve both high absorption and necessary voltage[6,7]. (2) Water is not necessarily split at a solar cell's maximum power point. Stacking more junctions to increase the photovoltage far above 1.8 V is therefore not useful. (3) At the semiconductor-liquid interface, conduction and valence bands need to be aligned in a way that the redox potential is located within the band gap and carrier transport into the electrolyte is promoted. The semiconductor-liquid interface may serve as Schottky-like contact to separate generated charge carriers. (4) (Photo-)Corrosion in the liquid must be minimized.

In Ref.[6] we calculated ideal tandem PV efficiences within the current-matched Shockley-Queisser limit and pointed out that the bandgaps of Si as a bottom cell and $GaP_{0.98}N_{0.02}$ as a lattice-matched top cell, 1.12 and 1.95 eV, respectively, are close to optimum. While adding As into a quaternary GaPNAs material would further decrease the bandgap of the top cell and thereby increase absorption efficiency[6], actual losses in the photovoltage of a tandem device must be considered additionally, so that $GaP_{0.98}N_{0.02}$/Si(100) with a total gap of about 3 eV is feasible for water splitting operation regarding sufficient voltage supply[24].

Besides adequate bandgaps, the band alignment relative to the redox potential of water is of importance to

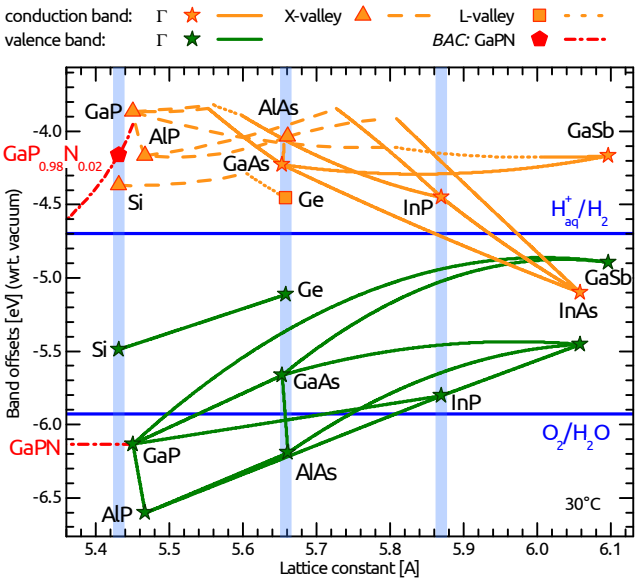

FIG. 1. Alignment of valence band maxima (green) and conduction band minima (orange) of various III-V compound semiconductors, their ternary compounds, and SiGe compounds relative to vacuum as a function of lattice constant. The line resp. symbol style indicates the type of the bandgap. Blue horizontal lines indicate the redox potential of water. Light blue vertical lines highlight the lattice constants of the common substrates Si, Ge/GaAs and InP. Data for 30 °C from Refs[25–30].

split water. As an update of the work by Tiwari and Frank[25], we estimated the band offsets of various III-V semiconductors, Ge and Si as well as their ternary respectively binary compounds in Fig.1. The values are a compilation of the lattice constants, bandgaps, valence band offsets (VBO) and bowing parameters given by Vurgaftman et al.[26] for the III-V compounds and for Si and Ge by Tiwari and Frank[25]. We assumed that the lattice constants of ternary III-V's and binary SiGe follow Vegard's law[31]. For the bandgap E_g and VBO of a compound of two materials A, B (with a fraction x of B), bowing in the form

$$\xi = (1-x)\,\xi_A + x\,\xi_B + x\,(1-x)\,\beta \qquad (2)$$

has to be considered[32], where ξ is either E_g or the VBO and β the according bowing parameter. The conduction band offset (CBO) is then given by CBO = E_g + VBO. For Ge, we assumed an average Ge/GaAs offset from Ref.[27] and kept the alignment of Si wrt. Ge from Ref.[25]. To include the redox potential of water, we transformed the band offsets relative to vacuum scale using the electron affinity of InP of 4.38 eV given in Ref.[29]. The work function of the H_2/H_2O potential against vacuum scale[30] is assumed to lie in the order of 4.7 eV with the O_2/H_2O potential 1.23 eV below that value. For III-V-N alloys, E_g is highly reduced already by small nitrogen incorporation[33] as can be described by the band anticrossing (BAC) model[34,35]. The BAC model assumes changes only in the conduction band, so that we applied the values tabulated by Vurgaftman and Meyer[28] to the CBO of GaPN only. It should be noted that Fig. 1 contains experimental values from different sources and can only give a rough idea of the relative band alignment since doping, band bending, strain and different interface formations will have an influence that is not taken into account here.

Fig. 1 shows that both oxygen and hydrogen evolution should be possible with GaP(N) while uncoated Si could evolve hydrogen only. To promote efficient transport to the liquid via band bending at the semiconductor-liquid interface, where the charge carriers are seperated, hydrogen should be evolved at the p-doped semiconductor side and oxygen at the n-doped side. This design, generally referred to as photochemical diode[36], significantly simplifies the device structure as the need for charge separation at p-n junctions is omitted. The band alignment in Fig. 1 suggests hydrogen evolution at a p-Si photocathode and an oxygen evolving photoanode at the n-GaPN side of a tandem photochemical diode interconnected with a tunnel junction. With an appropriate, pinhole-free protective layer such as Ni/NiO_x that protects the underlying Si[37], one could also imagine a reversed configuration with n-Si as photoanode and p-GaPN as photocathode. These two options for a tandem configuration enable more flexibility in the design of an appropriate tunnel junction, which might be included in the GaP nucleation buffer between the two subdiodes. A third, more conventional, hybrid approach could be the growth of the GaPN subdiode on a Si photovoltaic cell, providing bias for the water splitting reaction. As the monolithic stack has to be illuminated from the side with the larger band gap, the Si photovoltaic back side could be covered with an intransparent ohmic contact and a metal electrode, similar to previous III-V water splitting tandem realizations.[38]

IV. GAPN/SI(100) SURFACE PREPARATION

In Ref.[12], we showed that the initial formation of the GaP-water interface is strongly dependend on the atomic order at the GaP surface prior to water adsorption. In the following, we will discuss the MOVPE-preparation of GaPN/GaP/Si(100) surfaces in comparison to that of established GaP(100) respectively GaP/Si(100) surfaces. In principle, two well-defined surface reconstructions of GaP(100) can be prepared in MOVPE-ambient[15,16]: a "Ga-rich" (2×4) reconstructed surface–formed by mixed P-Ga dimers on top of a layer of Ga dimers–and a "P-rich" p(2×2) reconstructed surface. The latter consists of buckled P-dimers stabilized by one hydrogen atom per dimer and is often referred to as "(2×1)-like"[13]. Identical surface preparation may be applied to GaP/Si(100) surfaces[10]. In order to avoid P desorption from the surface at temperatures $T \gtrsim 480\,^{\circ}\mathrm{C}$, the surface is commonly stabilized by TBP supply during cooling after growth. Excess phosphorous and precursor residuals then desorb during the annealing step at 420 °C leading to formation of the well-ordered P-rich surface[10]. The Ga-rich surface is prepared by further annealing at 700 °C.

A. Ga-rich surface

Fig. 2(a) compares RA spectra of GaP/Si(100) and GaPN/GaP/Si(100) samples after Ga-rich preparation. The total GaP(N) film thickness for both samples is about 40 nm to minimize the difference in interference contributions to the spectra[40]. The minimum around 2.3 eV of the GaPN/GaP/Si(100) sample, which stems from the dimerized surface reconstruction, is blue-shifted about 50 meV with respect to GaP/Si(100) and about 1 RAS unit less intense. While both spectra match well at the maximum around 3 eV and beyond 3.9 eV, the lineshape around the E_1 transition is different (highlighted in yellow). A decreased amplitude of the minimum peak around 2.3 eV could be caused by both excess nitrogen (resp. precursor residuals) on the surface, a disordering effect by nitrogen incorporated into the surface or different anti-phase domain contents[41]. Anti-phase disorder as the origin of the reduced RAS peak intensity is unlikely, since we prepared almost single-domain Si(100) surfaces[8] prior to III-V growth and small residual anti-phase domains will annihilate during GaP growth. Accordingly, the LEED patterns in Fig. 2(b,c) show the (2×4) diffraction pattern expected for Ga-rich GaP(100) without signs of a mutually perpendicular structure. The spots and

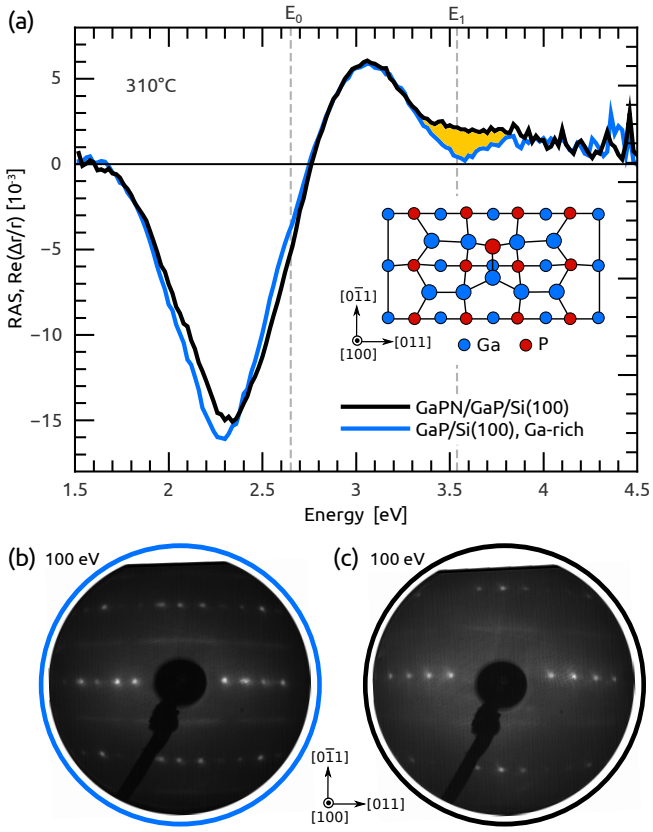

FIG. 2. (a) RA spectra of Ga-rich GaP/Si(100) (blue line) and GaPN/GaP/Si(100) (black line) measured at 310 °C. The difference between the spectra at E_1 (yellow area) is shown in detail in Fig. 3(b). Dashed gray lines indicate the critical point energies of GaP[39]. The inset sketches the (2×4) surface reconstruction of Ga-rich GaP(100). LEED pattern of (b) the Ga-rich GaP/Si(100) surface and (c) the GaPN/GaP/Si(100) surface from (a) after transfer to UHV.

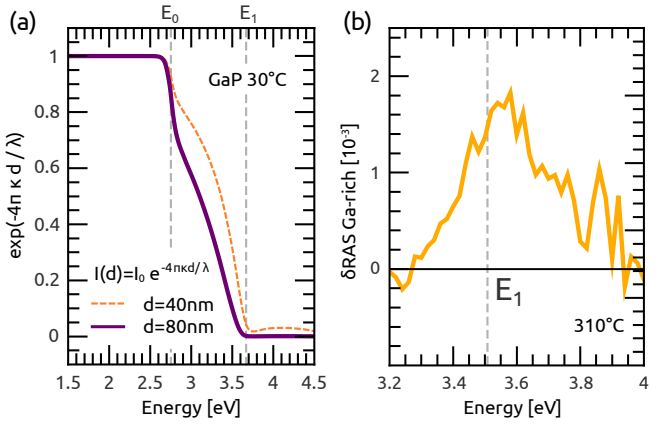

FIG. 3. (a) Transmission through GaP at room temperature according to Lambert-Beer's law with data from Ref.[42]. (b) Difference RA spectrum of GaPN/GaP/Si(100) and GaP/Si(100) around the E_1 transition of GaP[39].

especially the streaks along [011], however, are slightly brighter for the GaP/Si(100) sample (Fig. 2(b)) than for the GaPN/GaP/Si(100) sample (Fig. 2(c)), which could be caused by the incorprated N or excess atoms at the surface. Regarding the latter, we could not detect carbon (as signature of precursors residuals) on the GaPN/GaP/Si(100) surface with XPS so that excess nitrogen seems more likely. Furthermore, slight differences in the film thickness or modified interference modulation due to the GaPN/GaP interface[40] might influence the lineshape of the peak. In contrast, higher absorption beyond the E_1 transition will hinder interference. Fig. 3(a) displays the transmission factor $\exp(-4\pi\, d\, \kappa\, \lambda)$ of the Lambert-Beer law, $I(d,\lambda) = I_0 \exp(-4\pi\, d\, \kappa\, /\, \lambda)$, (where I is the fraction of an incident light intensity I_0 transmitted through a medium of thickness d with an imaginary part κ of the index of refraction), for GaP at room temperature (κ from data tabulated by Jellison[42]). For a 40 nm thick, heteroepitaxially grown GaP film, a fraction less than 5 % of the incoming light reaches the heterointerface (Fig. 3(a), dashed orange line) and—even if reflected 100 % at the heterointerface—will be absorbed in the GaP film after internal reflection (Fig. 3(a), violet line). This was also observed during thickness dependent GaP growth on Si(100)[40]. Therefore, we assume that interference caused by the GaP/Si(100) heterointerface is negligible here for the discussion of features in the RA spectra around and beyond the E_1 transition. Interpreting spectral features at the E_1 transition as caused by surface modified bulk transitions, the different lineshape around 3.5 eV probably is a signature of nitrogen incorporation into the GaP bulk. Fig. 3(b) depicts the difference of the GaPN/GaP/Si(100) and GaP/Si(100) spectra shown in Fig. 2 for Ga-rich preparation:

$$\delta\mathrm{RAS} = \left.\frac{\Delta r}{r}\right|_{\mathrm{GaPN/GaP/Si(100)}} - \left.\frac{\Delta r}{r}\right|_{\mathrm{GaP/Si(100)}} . \quad (3)$$

A peak-like structure located around E_1, similar to those observed for the linear electrooptic effect in GaAs[43], with a higher energetic shoulder is observed. We found that this feature exhibits a correlation to the amount of incorporated nitrogen which is subject to ongoing investigations.

The annealing step at 700 °C during Ga-rich preparation might in principle also lead to N depletion in the GaPN film. To check the nitrogen content, we performed XRD measurements on both samples. Fig. 4 shows the $\omega/2\theta$ scan and according fits relative to the Si(400) peak position of the substrate. Reciprocal space map measurements (not shown here) indicate that the GaP film is almost completely strained. Fitting the thickness fringes accordingly yields a GaP film thickness of about 39 nm as expected for the growth parameters used here[40]. The diffractogram of the GaPN/GaP/Si(100) sample can be fitted with good agreement yielding about 17 nm GaPN with 2.2 % of nitrogen and a GaP buffer thickness of about 16 nm. Nitrogen thus seems not to desorb remarkably from the bulk of the GaPN film, which is in line with

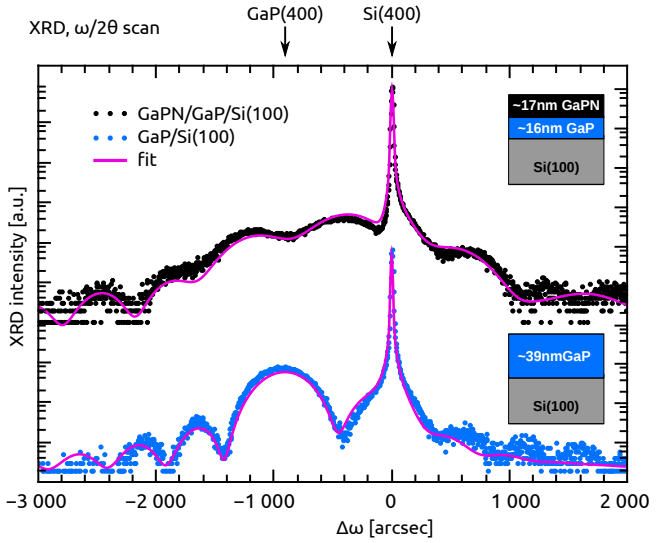

FIG. 4. $\omega/2\theta$ scan of GaP/Si(100) and GaPN/GaP/Si(100) relative to ω of Si(400). The fit yields the thicknesses indicated in the insets and a N content of 2.2 % in the GaPN epilayer. Arrows indicate the peak positions for Si(400) and pseudomorphic, not-relaxed GaP(400).[44]

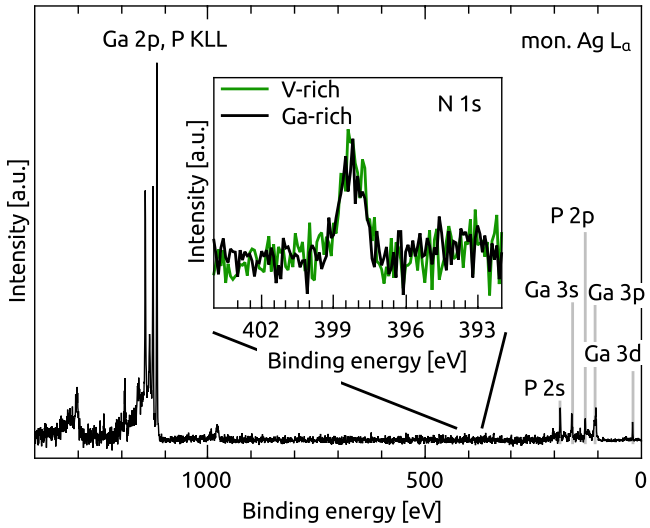

FIG. 5. XPS survey spectrum employing a monochromated Ag L_α source. The insets shows a detail spectrum of the N 1s emission of a V-rich sample prepared without UDMH stabilization after growth as well as the same sample after Ga-rich preparation.

Ref.[45] where sticking limited N incorporation is found for GaPN.

Since XRD (Fig.4) probes mainly the bulk, we applied XPS as a complementary method mainly sensitive to the surface nitrogen concentration. Monochromated Ag L_α X-rays ($h\nu = 2984.3$ eV) were used because, in contrast to Al K_α, the Ga LMM Auger lines are not superimposed to the N 1s photoemission line. The intensity of this source is, however, almost two orders of magnitude lower than the typically employed monochromated Al K_α source. Together with the nitrogen content of only $x \approx 0.02$ and the low cross-section of N 1s, this results in a relatively noisy signal when compared to Al K_α. We prepared a sample with higher N content and characterized it with XPS at first after V-rich preparation and a second time after Ga-rich preparation. The N 1s emission (inset of Fig. 5) does not decrease, further emphasizing that nitrogen is not lost during the annealing steps for the according surface preparation.

B. Group–V-rich surface

Nitrogen is incorporated inefficiently into GaP[45] so that UDMH:TPB ratios in the order of 1 are necessary to incorporate few percents of nitrogen. Fig. 6(a) compares the RA spectra of GaP/Si(100) (Fig. 6(a) blue line) and GaPN/GaP/Si(100)(Fig. 6(a) black line) measured at 310 °C after group–V-rich surface preparation including group–V stabilization after growth and annealing without precursor supply at 420 °C and 470 °C, respectively (the identical samples that were later prepared Ga-rich, see Fig. 2). After annealing at 420 °C without precursor supply, the intensity of the maximum around the E_1 transition of the GaPN/GaP/Si(100) was decreased drastically compared to GaP/Si(100) (not shown here). Further annealing at 470 °C lead to an increasing signal but still a factor of 1.7 less amplitude than the spectrum of the GaP/Si(100) surface (cf. gray line in Fig. 6(a)), i.e. significantly less than in the according Ga-rich case. The peak position is shifted about 70 meV towards blue. Again, both excess nitrogen (resp. precursor residuals) on the surface, an disordering effect by nitrogen incorporated into the surface and different antiphase domain contents[41] could in principle lead to the decreased amplitude. The latter is unlikely due to the increased amplitude after annealing at 470 °C respectively Ga-rich preparation (cf. Fig 2) and can be ruled out after contamination-free transfer to UHV: the LEED patterns of both samples, Fig. 6(b) and (c) respectively, show single-domain (2×1)-like diffraction patterns with a spot at half-order only along $[0\bar{1}1]$ direction—as was also expected for growth on almost single-domain Si(100) substrates[8]. The spots and, in particular, the streaks along $[0\bar{1}1]$, which are related to the c(4×2)-like order of buckled dimers and their flipping at room temperature[46], are less pronounced at the GaPN/GaP/Si(100) surface compared to GaP/Si(100) . This could once more be related to excess nitrogen or UDMH residuals adsorbed on the surface during stabilization. An implication of excess atoms at the surface could be that P-H bonds at the P-dimers are not as well ordered as for the P-rich GaP(100). The minimum in the RA spectrum of P-rich GaP(100) at about 2.3 eV originates in anisotropic transitions between surface states related to these P-H bonds[13]. The RA spectrum of the GaPN/GaP/Si(100) surface in Fig. 6 differs significantly at that minimum. Compared

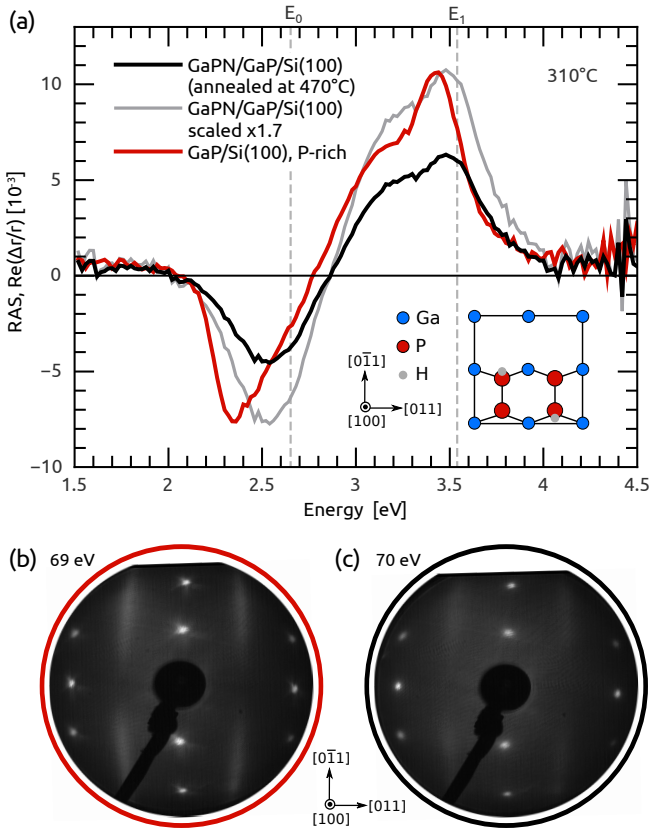

FIG. 6. (a) RA spectra of P-rich GaP/Si(100) (red line), GaPN/GaP/Si(100) after annealing at 470 °C without precursor supply (black line) and the latter scaled by 1.7 (gray line), all measured at 310 °C. Dashed gray lines indicate the critical point energies of GaP[39]. The inset sketches the p(2×2) surface reconstruction of P-rich GaP(100). LEED pattern of (b) the P-rich GaP/Si(100) surface and (c) the GaPN/GaP/Si(100) surface from (a) after transfer to UHV.

to GaP/Si(100), the peak is more symmetric, shifted about 200 meV towards the E_0 transition and less intense. This behaviour is similar to P-rich GaP(100) after water adsorption—probably modifying the P-H bonds—and subsequent annealing in nitrogen[12], where the peak shape of P-rich GaP(100) could only be restored when offering hydrogen to the surface. In XPS, we could not detect carbon (as signature of UDMH precursor residuals, see Fig. 5) on the GaPN/GaP/Si(100) surface so that excess nitrogen seems to be the origin of changes on the surface here. Since both spectra differ less after Ga-rich preparation, a pure interference effect caused by the GaPN/GaP heterointerface or the slightly different total film thickness is unlikely.

Annealing temperatures above 470 °C in order to prepare atomically well-defined group–V-rich GaPN(100) surfaces seem feasible since annealing at 700 °C does not lead to N depletion in the GaPN epilayer but to rather well-defined Ga-rich surfaces. Regarding group–V-rich preparation, temperatures above 490 °C are, however, critical since P can desorb from the surface[10]. Therefore we omitted UDMH stabilization after growth while cooling with TBP supply only. Fig. 7(a) compares the RA spectrum of GaPN/GaP/Si(100) (green line), prepared analogously as in Fig. 6 despite cooling with only TBP supply and subsequent annealing at 420 °C to desorb excess P, with the spectra shown in Fig. 6(a). The amplitude of the GaPN/GaP/Si(100) spectrum matches now almost that of GaP/Si(100) and the shift of the minimum peak ils drastically decreased (note that after 20 nm of GaP, the difference in anti-phase concentration of both GaPN/GaP/Si(100) samples was only about 5 % according to a semi-empirical approach[47]). The lineshape, however, is broader respectively more symmetric. The δRA spectrum (grey line) indicates a contribution at about the E_0 transition. While this could in principle caused by interference, it seems likely that either a N-modified bulk transition close to E_0 or the influence of nitrogen on the anisotropic surface state transition of P-rich GaP(100) causes this contribution. The growth of samples with different GaPN epilayer thicknesses and comparison to growth on GaP(100) could clarify this point in future studies. The shift of the maximum close to E_1 is hardly reduced by the changed surface preparation which indicates again a bulk-like contribution to the spectrum caused by nitrogen incorporation. The incorporated nitrogen could modify the E_1 bulk transition–as observed in the Ga-rich case–and thereby influence the surface modification of this transition to which the max-

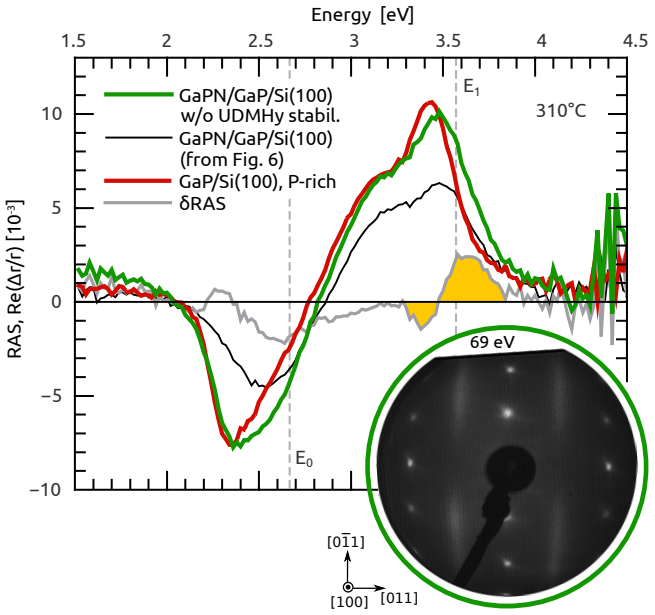

FIG. 7. RA spectra of P-rich GaP/Si(100) and GaPN/GaP/Si(100) from Fig. 6 and GaPN/GaP/Si(100) annealed at 420 °C after cooling with TBP supply only (black line), all measured at 310 °C. The difference between the spectra at E_1 is highlighted in yellow. Dashed gray lines indicate the critical point energies of GaP[39]. The inset shows the LEED pattern of GaPN/GaP/Si(100) cooled with TBP supply only.

imum of the P-rich GaP(100) RAS signal is ascribed. In agreement with the shift of the peak position, the δRA spectrum (highlighted in yellow) shows a derivative-like structure. This feature is superimposed by a peak-like structure at about E_1 similar to that observed for the Ga-rich surface in Fig. 3. Accordingly, this feature seems not to be related to a specific surface reconstruction supporting the interpretation as a bulk-like N contribution. The LEED pattern (inset Fig. 7) clearly shows the (2×1)-like reconstruction with both spots and streaks as bright as for P-rich GaP/Si(100) (inset Fig. 6(b)), indicating a well-ordered surface terminated with buckled dimers.

V. CONCLUSION

We compiled band offsets in III-V/IV heterostructures and proposed a photochemical diode based on a $GaP_{0.98}N_{0.02}$/Si(100) tandem with bandgaps close to optimum and band alignment suitable for direct photoelectrolysis. The atomic order at surfaces of GaP(100) is known to have great impact on the initial interface formation to water[12]. In order to grow smooth GaPN epilayers and to prepare well-defined surfaces similar to those of GaP(100), we monitored the whole GaPN/Si(100) growth process *in situ* with RAS. Stabilization with UDMH after GaPN growth leads to excess nitrogen at the surface, which cannot be removed during a standard P-rich preparation step. Annealing at higher temperatures leads to the Ga-rich GaPN/Si(100) surface and RAS signals of similar amplitude compared to GaP/Si(100). XPS and XRD showed that nitrogen is not desorbing considerably during the annealing procedure. The V-rich GaPN/Si(100) surface can be prepared when UDMH is switched off simultaneously with TEGa. The P-dimer related minimum in the RA spectrum of P-rich GaP(100) is broadened at V-rich GaPN/Si(100) surfaces, which is probably caused by nitrogen at the surface layers or a modified E_0 transition of GaP. RA spectra of both Ga-rich and V-rich GaPN/Si(100) surfaces contain an additional contribution at about the E_1 interband transition of GaP, which is believed to relate to nitrogen incorporation into the GaP bulk. The origin of this feature in the *in situ* RAS signals is subject to ongoing investigations.

VI. ACKNOWLEDGEMENTS

The Authors would like to thank M. Schmidtbauer, L. Spieß, and K. Tonisch for advice regarding the XRD analysis as well as H. Döscher for discussions regarding the band alignment. This work was supported by the BMBF (project no. 03SF0404A). MM. May and H. Stange acknowledge scholarships of the Studienstiftung des deutschen Volkes e.V. This material is based upon work performed by the Joint Center for Artificial Photosynthesis, a DOE Energy Innovation Hub, as follows: parts of the organization of the work, of the discussion as well as of the manuscript wording and composition were supported through the Office of Science of the US Department of Energy under Award No. DE-SC0004993.

[1] M. A. Green, K. Emery, Y. Hishikawa, W. Warta, and E. D. Dunlop, Progress in Photovoltaics: Research and Applications **21**, 1 (2013).
[2] F. Dimroth, M. Grave, P. Beutel, U. Fiedeler, C. Karcher, T. N. D. Tibbits, E. Oliva, G. Siefer, M. Schachtner, A. Wekkeli, A. W. Bett, R. Krause, M. Piccin, N. Blanc, C. Drazek, E. Guiot, B. Ghyselen, T. Salvetat, A. Tauzin, T. Signamarcheix, A. Dobrich, T. Hannappel, and K. Schwarzburg, Progress in Photovoltaics: Research and Applications **submitted** (2013).
[3] G. A. Olah, G. K. S. Prakash, and A. Goeppert, Journal of the American Chemical Society **133**, 12881 (2011).
[4] B. Kaiser, D. Fertig, J. Ziegler, J. Klett, S. Hoch, and W. Jaegermann, ChemPhysChem **13**, 3053 (2012).
[5] W. Shockley and H. J. Queisser, Journal of Applied Physics **32**, 510 (1961).
[6] H. Döscher, O. Supplie, M. M. May, P. Sippel, C. Heine, A. G. Muñoz, R. Eichberger, H.-J. Lewerenz, and T. Hannappel, ChemPhysChem **13**, 2899 (2012).
[7] S. Hu, C. Xiang, S. Haussener, A. D. Berger, and N. S. Lewis, Energy Environ. Sci. **6**, 2984 (2013).
[8] S. Brückner, H. Döscher, P. Kleinschmidt, O. Supplie, A. Dobrich, and T. Hannappel, Physical Review B **86**, 195310 (2012).
[9] S. Brückner, P. Kleinschmidt, O. Supplie, H. Döscher, and T. Hannappel, New Journal of Physics **15**, 113049 (2013).
[10] H. Döscher and T. Hannappel, Journal of Applied Physics **107**, 123523 (2010).
[11] T. G. Deutsch, J. L. Head, and J. A. Turner, Journal of The Electrochemical Society **155**, B903 (2008).
[12] M. M. May, O. Supplie, C. Höhn, R. van de Krol, H.-J. Lewerenz, and T. Hannappel, New Journal of Physics **15**, 103003 (2013).
[13] P. H. Hahn, W. G. Schmidt, F. Bechstedt, O. Pulci, and R. D. Sole, Physical Review B **68**, 033311 (2003).
[14] W. Schmidt, J. Bernholc, and F. Bechstedt, Applied Surface Science **166**, 179 (2000).
[15] N. Esser, W. Schmidt, J. Bernholc, A. Frisch, P. Vogt, M. Zorn, M. Pristovsek, W. Richter, F. Bechstedt, T. Hannappel, and S. Visbeck, Journal of Vacuum Science & Technology B **17**, 1691 (1999).
[16] L. Töben, T. Hannappel, K. Möller, H. Crawack, C. Pettenkofer, and F. Willig, Surface Science **494**, L755 (2001).
[17] P. Sippel, O. Supplie, M. M. May, R. Eichberger, and T. Hannappel, Phys. Rev. B **under review** (2013).
[18] T. Hannappel, S. Visbeck, L. Töben, and F. Willig, Review of Scientific Instruments **75**, 1297 (2004).
[19] P. Weightman, D. S. Martin, R. J. Cole, and T. Farrell, Reports on Progress in Physics **68**, 1251 (2005).
[20] W. Ayers, *Photolytic Production of Hydrogen*, US Patent No. 4,466,869 (1984).
[21] R. E. Rocheleau, E. L. Miller, and A. Misra, Energy & Fuels **12**, 3 (1998).
[22] S. Y. Reece, J. A. Hamel, K. Sung, T. D. Jarvi, A. J. Esswein, J. J. H. Pijpers, and D. G. Nocera, Science **334**, 645 (2011).
[23] B. Kaiser, W. Jaegermann, S. Fiechter, and H.-J. Lewerenz, Bunsen-Magazin **4**, 104 (2011).
[24] T. Hannappel, M. M. May, and H.-J. Lewerenz, in *Photoelectrochemical Water Splitting: Materials, Processes and Architectures*, edited by H.-J. Lewerenz and L. Peter (The Royal Society of Chemistry, 2013) pp. 223–265.
[25] S. Tiwari and D. J. Frank, Applied Physics Letters **60**, 630 (1992).
[26] I. Vurgaftman, J. R. Meyer, and L. R. Ram-Mohan, Journal of Applied Physics **89**, 5815 (2001).
[27] A. Franciosi and C. G. V. de Walle, Surface Science Reports **25**, 1 (1996).
[28] I. Vurgaftman and J. R. Meyer, Journal of Applied Physics **94**, 3675 (2003).

[29]T. E. Fischer, Physical Review **142**, 519 (1966).
[30]W. N. Hansen and D. M. Kolb, Journal of Electroanalytical Chemistry and Interfacial Electrochemistry **100** (1979).
[31]L. Vegard, Zeitschrift für Physik **5**, 17 (1921).
[32]J. A. Van Vechten and T. K. Bergstresser, Physical Review B **1**, 3351 (1970).
[33]M. Weyers, M. Sato, and H. Ando, Japanese Journal of Applied Physics **31**, L853 (1992).
[34]W. Shan, W. Walukiewicz, J. W. Ager, E. E. Haller, J. F. Geisz, D. J. Friedman, J. M. Olson, and S. R. Kurtz, Physical Review Letters **82**, 1221 (1999).
[35]J. Wu, W. Walukiewicz, K. M. Yu, J. W. Ager, E. E. Haller, Y. G. Hong, H. P. Xin, and C. W. Tu, Physical Review B **65**, 241303 (2002).
[36]A. J. Nozik and R. Memming, The Journal of Physical Chemistry **100**, 13061 (1996).
[37]M. J. Kenney, M. Gong, Y. Li, J. Z. Wu, J. Feng, M. Lanza, and H. Dai, Science **342**, 836 (2013).
[38]O. Khaselev and J. A. Turner, Science **280**, 425 (1998).
[39]S. Zollner, M. Garriga, J. Kircher, J. Humlícek, M. Cardona, and G. Neuhold, Thin Solid Films **233**, 185 (1993).
[40]O. Supplie, T. Hannappel, M. Pristovsek, and H. Döscher, Physical Review B **86**, 035308 (2012).
[41]H. Döscher, T. Hannappel, B. Kunert, A. Beyer, K. Volz, and W. Stolz, Applied Physics Letters **93**, 172110 (2008).
[42]G. Jellison Jr., Optical Materials **1**, 151 (1992).
[43]S. E. Acosta-Ortiz and A. Lastras-Martínez, Physical Review B **40**, 1426 (1989).
[44]O. Skibitzki, F. Hatami, Y. Yamamoto, P. Zaumseil, A. Trampert, M. A. Schubert, B. Tillack, W. T. Masselink, and T. Schroeder, Journal of Applied Physics **111**, 073515 (2012).
[45]B. Kunert, J. Koch, T. Torunski, K. Volz, and W. Stolz, Journal of Crystal Growth **272**, 753 (2004).
[46]P. Kleinschmidt, H. Döscher, P. Vogt, and T. Hannappel, Physical Review B **83**, 155316 (2011).
[47]H. Döscher, B. Kunert, A. Beyer, O. Supplie, K. Volz, W. Stolz, and T. Hannappel, Journal of Vacuum Science & Technology B **28**, C5H1 (2010).